JOURNAL OF COMPUTATIONAL PHYSICS 90, 176–199 (1990)

Numerical Solution of the Hele–Shaw Equations*

NATHANIEL WHITAKER†

Lawrence Berkeley Laboratory and Department of Mathematics, University of California, Berkeley California 94720

Received August 26, 1987; revised October 27, 1989

An algorithm is presented for approximating the motion of the interface between two immiscible fluids in a Hele–Shaw cell. The interface is represented by a set of volume fractions. We use the simple line interface calculation method along with the method of fractional steps to transport the interface. The equation of continuity leads to a Poisson equation for the pressure. The Poisson equation is discretized. Near the interface where the velocity field is discontinuous, the discretization is based on a weak formulation of the continuity equation. Interpolation is used on each side of the interface to increase the accuracy of the algorithm. The weak formulation as well as the interpolation are based on the computed volume fractions. This treatment of the interface is new. The discretized equations are solved by a modified conjugate gradient method. Surface tension is included and the curvature is computed through the use of osculating circles. For perturbations of small amplitude, a good agreement is found between the numerical results and linearized perturbation theory. Numerical results are presented for the finite amplitude growth of unstable fingers.

1. INTRODUCTION

In this paper, we present a numerical method for evolving an interface between two immiscible fluids in a Hele–Shaw cell (two closely placed parallel plates). These fluids are immiscible in the sense that there is a finite surface tension which stabilizes small-scale disturbances in the interface. The equations describing the flow of a fluid in a Hele–Shaw cell are the equation of motion

$$\mathbf{u} = -\frac{b^2}{12\mu}\nabla p \tag{1}$$

and the equation of continuity

$$\nabla \cdot \mathbf{u} = 0, \tag{2}$$

* This work was supported in part by the Applied Mathematics Sciences Subprogram of the Office of Energy Research, U.S. Department of Energy under Contract DE-AC03-76SF00098, and in part by IBM while the author held an IBM graduate fellowship. This paper is a condensed version of [34], the author's Ph. D. dissertation in the U.C. Berkeley Mathematics Department.

† Present address: Department of Mathematics, University of Massachusetts, Amherst, MA 01003.

0021-9991/90 $3.00

where μ is the fluid viscosity, b is the spacing between the plates in the Hele–Shaw cell. The plates are taken as horizontal, the positive y-axis is in the direction of the flow, the x-axis is parallel to the plates, and the z-axis is perpendicular to the plates. The velocity vector $\mathbf{u}$ has two components u and v which are functions of t (time), x and y. These velocities result from taking an average of the three-dimensional velocity field. The pressure p is also an averaged pressure.

Derivations of the equations are found in Lamb [20] and Bear [2]. An introduction to the above problem is found in [32] along with a dimensionless form of the equations.

The problem of tracking an interface in a Hele–Shaw cell is of interest for many reasons. When one fluid displaces another fluid in a porous medium, the interface between the two fluids can be stable or unstable. For an unstable interface, small disturbances in an initially horizontal interface grow into long *fingers*. This instability is of interest, for example, in secondary oil recovery where residual oil is forced out of the ground by the injection of another fluid, usually water. Some numerical models to evolve interfaces between two fluids in a porous medium are presented by Concus and Proskurowski [10], Glimm *et al.* [15, 16], Lotstedt [22], Chorin [4], and Colella *et al.* [8].

Usually these interfaces are three-dimensional and the equations describing them are nonlinear, making them difficult to study both experimentally and analytically. The Hele–Shaw cell is often used as a device for studying two-dimensional flow in porous medium. This is due to the fact that the differential equations for the velocity field in a porous medium are the same equations for the velocity field in a Hele–Shaw cell, apart from scaling. In addition, the Hele–Shaw cell is also a simple system which is easier to vizualize than a porous medium.

In a Hele–Shaw cell, for horizontal flow, an interface becomes unstable when a less viscous fluid displaces a more viscous fluid. Unstable fingering in a Hele–Shaw cell has been studied experimentally by many authors (see Saffman and Taylor [30]; Chuoke *et al.* [7]; Gupta *et al.* [18]; White *et al.* [35, 36]; Pitts [29]; Park *et al.* [27]). Saffman and Taylor performed a linearized stability analysis for an initially flat interface and found an analytic solution for the shape of single fingers neglecting surface tension. McLean and Saffman [23] found an analytic shape of single fingers including surface tension. Chuoke *et al.* [7] performed experiments in a Hele–Shaw cell and in packed bed models. They also performed a linearized stability analysis for an initially flat interface. Paterson [28] recently performed experiments investigating radial fingering, i.e., an initially circular interface is perturbed and fingering occurs. Paterson argues that the radial model is more appropriate to practical situations.

In this paper we present a numerical method which demonstrates high accuracy in evolving interfaces represented by waves of small amplitude thereby suggesting that it gives reasonable results for large amplitude waves. To the author's knowledge, numerical methods simulating the evolution of an interface in a Hele–Shaw cell have been presented by Meng and Thomson [25], by Tryggvason and Aref [32, 33], by Degregoria and Schwartz [11, 12], and by Meiburg and Homsy

[24]. Tryggvason and Aref develop and use a vortex method to evolve this interface. The results seem to agree well with those of the linearized theory and the steady fingers of McLean and Saffman [23]. In their method, the authors represent the interface as a vortex sheet and derive an equation for its strength which they solve. They evolve this sheet using the vortex-in-cell method as presented by Christensen in [6]. Meiburg and Homsy also represent their interface as a vortex sheet but they discretize it into circular arcs. Their results compare well with analytical results of McLean and Saffman [23] and other solutions given by Aitchison and Howison [1]. Degregoria and Schwartz develop and use a boundary-integral technique. Their results also compare well with the steady fingers of McLean and Saffman [23] and seem to be excellent for small values of the surface tension. The purpose of this paper is not to give a comparison of the author's method with the above methods but to present a new method. This method uses some new techniques and gives some interesting results. This approach could be used in similar problems. We compared our numerical method extensively with the predictions of the linearized theory and the results are surprizingly good. This gives us some indication of how well our numerical method might expect to handle unstable interfaces, which evolve into fingers. Some of these evolved interfaces are presented here and they compare well qualitatively with those obtained experimentally and numerically by other authors.

The method we use to transport the interface, the simple line interface method (SLIC), is presented initially by Noh and Woodward in [26]. Chorin, in [3], modifies this method to increase accuracy and applies it to flame propagation. Lotstedt, in [22], makes further modifications to increase accuracy in solving Burgers' equation and two phase porous flow. Sethian [31] and Ghoniem *et al.* [13] use SLIC to attain highly successful results in combustion. SLIC relies on local reconstructions of the interface and is highly effective in handling interfaces with such complex geometry as fingers and cusps. We present a method for finding the velocity field by discretizing a weak formulation of the continuity equation, Eq. (2). Interpolation is used to increase accuracy. A modified conjugate gradient method is used to solve the system resulting from the discretization. Curvature is computed using a method presented by Chorin in [5]. This curvature is then used to include surface tension.

The remainder of this paper is organized in the following way. In Section 2, we give a formulation of the problem that we are solving. In Section 3, we present our numerical method. In Section 4, we show how the rate of growth of a wave of small amplitude is calculated by our numerical method. The numerical results are then compared with the results as predicted by the linearized theory in various tables and graphs. In Section 5, we show the evolution of unstable interfaces for long periods of time and Section 6 is devoted to a general discussion of the results and our conclusions about the method.

2. Formulation of the Problem

In this section, we give the formulation of the problem which we solve numerically. In the derivation of the equations describing the flow of a fluid in a Hele–Shaw cell, $\partial p/\partial z = 0$, implying that p is a function of x and y only. The velocity field $\mathbf{u} = (u, v)$ is an averaged velocity field which is also a function of x and y only. The flow is considered as two dimensional in the $x-y$ plane. We consider the flow to lie in a rectangular box R with width a and height c (see Fig. 1). All functions defined on the box are periodic in the horizontal direction with period a. Black fluid flows into the box from behind the interface at a constant velocity $(0, V)$ across the line segment between the points $(0, 0)$ and $(a, 0)$. White fluid flows out of the box in front of the interface at a constant velocity $(0, V)$ across the line segment between the points $(0, c)$ and (a, c). The region in which the black fluid lies is RB and the region in which the white fluid lies is RW such that the union of those regions is the region R. We are interested in the evolution of the interface between the white and the black fluids with viscosities μ_w and μ_b, respectively. Our numerical method is designed to solve the following problems subject to the following conditions.

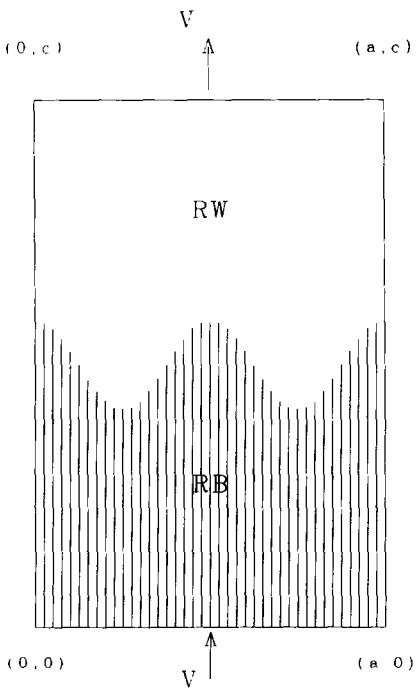

Fig. 1. Typical interface.

In *RW*, find a solution to the equations

$$\mathbf{u}_w = -\frac{b^2}{12\mu_w}\nabla p_w \tag{3}$$

$$\nabla \cdot \mathbf{u}_w = 0 \tag{4}$$

such that the velocity, $v_w(x, c)$, is prescribed.

In *RB*, find a solution to the equations

$$\mathbf{u}_b = -\frac{b^2}{12\mu_b}\nabla p_b \tag{5}$$

$$\nabla \cdot \mathbf{u}_b = 0 \tag{6}$$

such that the velocity, $v_b(x, 0)$, is prescribed.

These two problems are connected by the following conditions:

(1) The Rankine–Hugoniot condition is satisfied at the interface, i.e.,

$$\mathbf{u}_w \cdot \mathbf{n} - \mathbf{u}_b \cdot \mathbf{n} = 0, \tag{7}$$

where $\mathbf{n}$ is the normal to the interface pointing towards the black fluid.

(2) Surface tension is included in this model by specifying a jump in the pressure across the interface given by

$$p_w(x_0, y_0) - p_b(x_0, y_0) = -\tau / R_{x_0, y_0}, \tag{8}$$

where $p_b(x_0, y_0)$ is the limit of $p_b(x, y)$ as (x, y) approaches (x_0, y_0) with (x, y) a point in the black fluid and p_w similarly defined, τ is the surface tension, and R_{x_0, y_0} is the signed radius of curvature of the interface at the point (x_0, y_0).

(3) The compatibility condition

$$\int_0^a v_b(x, 0)\, dx = \int_0^a v_w(x, c)\, dx, \tag{9}$$

is satisfied; i.e., the inflow velocity and the outflow velocity cannot be specified arbitrarily.

After finding the velocity field above, we advect the black and white fluids in such a way that the interface is transported.

3. Numerical Method

In Section 3.1, it is shown how the interface is transported with the simple line interface calculation (SLIC) method. In Section 3.2, our method for calculating the velocity field is presented. The interface is reconstructed and the reconstruction is

used to discretize a weak formulation of the continuity equation. After the discretization of the continuity equation, a system of equations results and these equations are solved by a modified conjugate gradient method presented in Section 3.3. In Section 3.4, it is explained how curvature is calculated and how surface tension is included.

3.1. *SLIC*

Consider the two-fluid flow in the rectangular box described in Section 2 and a numerical grid of uniform mesh size h imposed over this box. The centers of the cells are located at the points (ih, jh), where i, j are integers and h is a small parameter. Assign a number $f_{i,j}$ to each cell equal to the fraction of black fluid in that cell. A cell (i, j) has volume fraction $f_{i,j}=1$ when it lies entirely behind the interface, volume fraction $f_{i,j}=0$ when it lies entirely in front of the interface and $0<f_{i,j}<1$ when the interface passes through the cell.

We wish to transport the black fluid over a time step k with a given velocity field $\mathbf{u}=(u, v)$. To accomplish this, the interface between the black and white fluids in each cell is reconstructed from the given volume fractions $f_{i,j}$. Each reconstruction is based on an inspection of the volume fractions, $f_{i,j}$, in the cell and its neighbors: the possible interfaces include horizontal interfaces, vertical interfaces, corners, and thin fingers as used by Chorin in [3]. The interface is then transported using the method of fractional steps. The black fluid is transported in the x direction with velocity u, the white fluid is then transported in the y direction with velocity v and the volume fractions are updated.

3.2. *Calculation of the Velocity Field*

The interface is reconstructed locally in each cell by comparing the volume fractions in the cell with those of its neighbors. The possible interfaces allowed in a cell include horizontal lines, vertical lines, and corners. This is done in a manner similar to that in SLIC. Below, we give the possible sets of volume fractions for cell (i, j) and its neighbors that we considered and the type of interface corresponding to each of these.

1. *Horizontal interface.* The interface is a horizontal line and is located at $y=(j-0.5)h+f_{i,j}h$. This case occurs, for example when; $0<f_{i,j}<1$, $f_{i,j-1}=1$, $f_{i,j+1}=0$, with $f_{i-1,j}>0$ and $f_{i+1,j}>0$ (see Fig. 2). The other cases are obtained by interchanging the roles of top and bottom and/or the roles of black and white.

2. *Vertical interface.* These cases are simply a rotation of the cases above for the horizontal interface.

3. *Corner.* This interface consists of a horizontal and vertical line meeting in the cell. This case occurs, for example when; $0<f_{i,j}<1$, $0<f_{i+1,j}<1$, $0<f_{i,j-1}<1$, $f_{i-1,j}=0$, and $f_{i,j+1}=0$ (see Fig. 3). The horizontal dimension a and vertical dimension b for this corner are determined by solving the equations

$$\frac{a}{b}=\frac{f_{i,j-1}}{f_{i+1,j}} \tag{10}$$

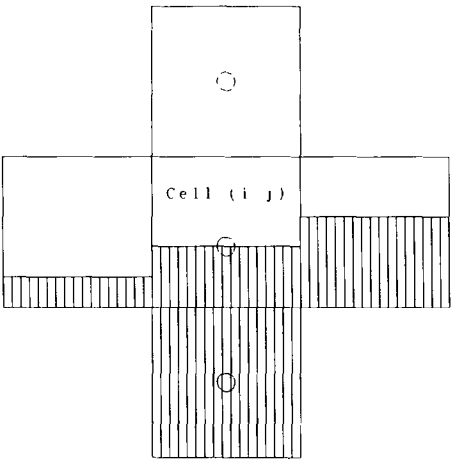

FIG. 2. Horizontal interface. Circles denote location in cell where pressure is solved for.

and

$$ab = f_{i,j}h^2 \tag{11}$$

for a and b as in the version of SLIC given by Chorin in [3]. The other cases are obtained by interchanging the roles of black and white, of top and bottom, and of left and right.

4. *Vertex corner.* This interface consists of two lines emanating from opposite vertices of cell (i, j) and intersecting at some point on the diagonal

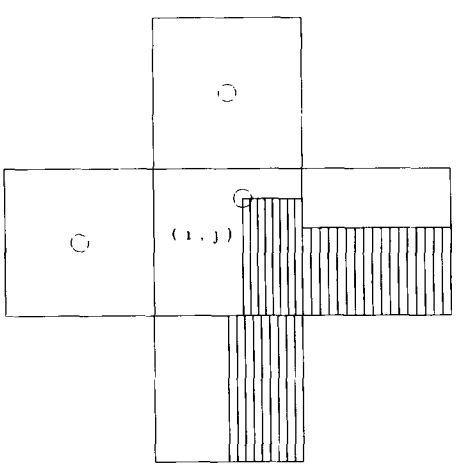

FIG. 3. Corner interface. Circles denote location in cell where pressure is solved for.

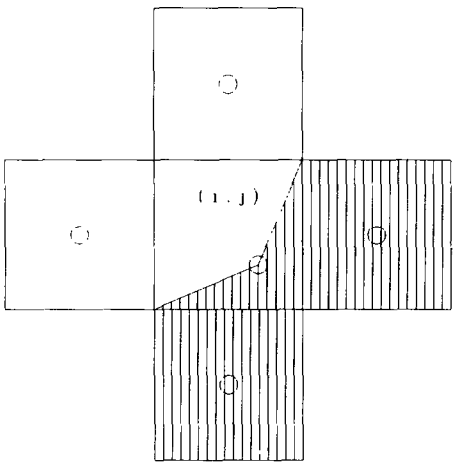

FIG. 4. Vertex interface. Circles denote location in cell where pressure is solved for.

through the other two vertices. The point of intersection is determined such that cell (i, j) contains volume fraction $f_{i,j}$. This case occurs, for example, when $0 < f_{i,j} < 1$, $f_{i+1,j} = 1$, $f_{i,j-1} = 1$, $f_{i-1,j} = 0$, $f_{i,j+1} = 0$ (see Fig. 4). The other cases are obtained by interchanging the roles of black and white and of left and right.

Given these reconstructions, we solve for the pressure $p_{i,j}$ at some point $\mathbf{z}_{i,j}$ in cell (i, j) whose location depends on the local reconstruction in that cell. For horizontal and vertical interfaces $\mathbf{z}_{i,j}$ is located on the interface, in the middle (see Fig. 2). For the corner, $\mathbf{z}_{i,j}$ is located at the point where the vertical and horizontal lines meet (see Fig. 3). For a vertex corner, $\mathbf{z}_{i,j}$ is located at the point on the interface where the two lines intersect the diagonal (see Fig. 4). For the case when cell (i, j) contains no interface $\mathbf{z}_{i,j}$ is located at the center of the cell.

An equation for each cell (i, j) in terms of the grid function's value, $p_{i,j}$, in cell (i, j) and the grid function's values in neighboring cells is obtained through the discretization of

$$\int_{\partial c_{i,j}} \mathbf{u} \cdot \mathbf{n} \, ds = 0, \tag{12}$$

where $\partial c_{i,j}$ is the boundary of the cell (i, j), $\mathbf{u}$ is the velocity field, and $\mathbf{n}$ is the outward normal. Equation (12) is a weak formulation of (2) and can be rewritten as

$$\int_{RS} \mathbf{u} \cdot \mathbf{n} \, ds + \int_{TS} \mathbf{u} \cdot \mathbf{n} \, ds + \int_{LS} \mathbf{u} \cdot \mathbf{n} \, d + \int_{BS} \mathbf{u} \cdot \mathbf{n} \, ds = 0, \tag{13}$$

where RS is the line segment on the right side of cell (i, j), TS is the line segment on the top side of cell (i, j), LS is the line segment on the left side of cell (i, j), and BS is the line segment on the bottom side of cell (i, j). Each of the four parts in (13)

above is approximated by the length of the line times $\mathbf{u}\cdot\mathbf{n}$ approximated at a convenient point on the line of integration.

When the interface crosses a cell, the line integral along each side is divided additionally into a part corresponding to the white fluid and a part corresponding to the black fluid, where each part is approximated in the same way. To approximate the length of the line for these situations, we need to approximate where the interface crosses the side. In general, the interface is estimated to cross a side at an average of where the local interfaces in the two cells sharing the side cross. For the case where one of the cells sharing the side is full of the white (black) fluid, no interface crosses the side only white (black) fluid.

Approximating $\mathbf{u}\cdot\mathbf{n}$ along the sides of the cell is equivalent to approximating $\partial p/\partial x$ along the vertical sides and $\partial p/\partial y$ along the horizontal sides of the cell (see Eqs. (3) and (5)). Suppose that $\partial p/\partial y$ is to be approximated along the top side of cell (i, j). In general, we would like to use a difference quotient as the approximation equaling the value of the grid function $p_{i,j+1}$ in cell $(i, j+1)$ minus the value of the grid function $p_{i,j}$ in cell (i, j) divided by the distance between the locations of the grid points in the two cells. However, when an interface passes through either cell (i, j) or $(i, j+1)$, $\mathbf{z}_{i,j}$ and $\mathbf{z}_{i,j+1}$ might not have the same x-coordinate. Linear interpolation is used to approximate the value of the grid function in cell (i, j) or $(i, j+1)$ at a point which has the same x-coordinate as the location of the grid function in cell $(i, j+1)$ or (i, j), respectively. This approximation of the grid function is then used in the difference quotient. The choice of the cells used in interpolation depends on the locations of $p_{i,j}$ and $p_{i,j+1}$, and in what fluid $\partial p/\partial y$ is being approximated. $\partial p/\partial x$ is approximated in the same manner. The above discretization at the interface for ∇p allows curvature to be incorporated easily (see Section 3.4). A complete description of the exact interpolation used for each situation can be found in [34]. The discretization of (13) can be thought of as a weak discrete divergence.

The equations for the cells along the boundary of the rectangular box are modified slightly due to the boundary conditions.

The case that occurs most frequently is the one where (i, j), $(i-1, j)$, $(i+1, j)$, $(i, j-1)$, and $(i, j+1)$ contain no interfaces and contain the same fluid. Without loss of generality, we assume the fluid in these cells to be black. The pressures are all cell centered and (13) can be approximated as follows:

$$h\kappa_b \frac{\partial p((i+0.5)h, jh)}{\partial x} + h\kappa_b \frac{\partial p(ih, (j+0.5)h)}{\partial y}$$

$$- h\kappa_b \frac{\partial p((i-0.5)h, jh)}{\partial x} - h\kappa_b \frac{\partial p(ih, (j-0.5)h)}{\partial y} = 0, \tag{14}$$

where $\kappa_b = -b^2/12\mu_b$.

Using the centered difference approximation, (14) can be approximated by

$$h\kappa_b \frac{p_{i+1,j} - p_{i,j}}{h} + h\kappa_b \frac{p_{i,j+1} - p_{i,j}}{h}$$

$$- h\kappa_b \frac{p_{i,j} - p_{i-1,j}}{h} - h\kappa_b \frac{p_{i,j} - p_{i,j-1}}{h} = 0, \tag{15}$$

which simplifies into the standard five-point difference formula for the Laplacian,

$$p_{i+1,j} + p_{i,j+1} + p_{i-1,j} + p_{i,j-1} - 4p_{i,j} = 0. \tag{16}$$

The following example illustrates the discretization of each term in Eq. (13) for a cell (i, j) with a horizontal interface passing through it (see Fig. 5). In this example, we assume zero surface tension, i.e., the pressure at the interface is single-valued. Section 3.4 explains how surface tension is included. This example uses the following set of volume fractions: $0 < f_{i-1,j} < 1$, $0 < f_{i,j} < 1$, $0 < f_{i+1,j} < 1$, $f_{i-1,j-1} = 1$, $f_{i,j-1} = 1$, $f_{i+1,j-1} = 1$, $f_{i-1,j+1} = 0$, $f_{i,j+1} = 0$, $f_{i+1,j+1} = 0$. It is assumed that $f_{i-1,j} \leqslant f_{i,j} \leqslant f_{i+1,j}$. By the rationale above, cells $(i-1, j)$, (i, j), and $(i+1, j)$ each contain a horizontal interface while the remaining cells given contain no interface. The points $\mathbf{z}_{i-1,j-1}$, $\mathbf{z}_{i,j-1}$, $\mathbf{z}_{i+1,j-1}$, $\mathbf{z}_{i-1,j+1}$, $\mathbf{z}_{i,j+1}$, and $\mathbf{z}_{i+1,j+1}$ are located in the center of their cells, since their cells contain no interface. The points $\mathbf{z}_{i-1,j}$, $\mathbf{z}_{i,j}$, and $\mathbf{z}_{i+1,j}$ are located at the centers of the horizontal interfaces. We denote the location of these points in each cell by a circle.

Let us first approximate the line integral on the right side of cell (i, j). The interface crosses the right side of cell (i, j) at the average of the two local interfaces, i.e., at $y = (j-0.5)h + 0.5h(f_{i,j} + f_{i+1,j})$. Since an interface crosses the right side of cell (i, j), the line integral along the right side is divided into two parts, one pertaining to the white fluid and one pertaining to the black fluid which is given by

$$\int_{RS} \mathbf{u} \cdot \mathbf{n}\, ds = \int_{RS(\text{white})} \mathbf{u} \cdot \mathbf{n}\, ds + \int_{RS(\text{black})} \mathbf{u} \cdot \mathbf{n}\, ds. \tag{17}$$

On the right-hand side of Eq. (17), $\mathbf{u} \cdot \mathbf{n}$ simplifies into $\kappa_w(\partial p((i+0.5)h, y)/\partial x)$ when $((i+0.5)h, y)$ lies in the white fluid and into $\kappa_b(\partial p((i+0.5)h, y)/\partial x)$ when $((i+0.5)h, y)$ lies in the black fluid where $\kappa_b = -b^2/12\mu_b$ and $\kappa_w = -b^2/12\mu_w$. The line integrals on the right side of Eq. (17) are approximated by $\mathbf{u} \cdot \mathbf{n}$ at some convenient point on the line times the length of the line. Using this and Eq. (17), we have the approximations,

$$\int_{RS} \mathbf{u} \cdot \mathbf{n}\, ds \approx 0.5h(f_{i,j} + f_{i+1,j})\, \kappa_b \frac{\partial p((i+0.5)h, \xi_1)}{\partial x}$$

$$+ (h - 0.5h(f_{i,j} + f_{i+1,j}))\, \kappa_w \frac{\partial p((i+0.5)h, \xi_2)}{\partial x}, \tag{18}$$

where ξ_1 and ξ_2 are the y-coordinates of convenient points on the right-hand side of cell (i, j) in the black and white fluids, respectively. The term $\partial p((i+0.5)h, \xi_1)/\partial x$ in Eq. (18) is approximated by the difference quotient

$$\frac{\tilde{p}_{i+1,j} - p_{i,j}}{d(\tilde{\mathbf{z}}_{i+1,j} - \mathbf{z}_{i,j})}, \tag{19}$$

where $\tilde{p}_{i+1,j}$ represents an approximation to the grid function at $\tilde{\mathbf{z}}_{i+1,j}$, a point in the black fluid, chosen on the line between $\mathbf{z}_{i+1,j}$ and $\mathbf{z}_{i+1,j-1}$, with the same y-coordinate as $\mathbf{z}_{i,j}$. The location of $\tilde{\mathbf{z}}_{i+1,j}$ is denoted by the diamond in Fig. 5 in cell $(i+1, j)$. $d(x, y)$ represents the Euclidean distance between the poiints x and y. We then interpolate linearly between $p_{i+1,j}$ and $p_{i+1,j-1}$ to approximate the grid functions value $\tilde{p}_{i+1,j}$ at $\tilde{\mathbf{z}}_{i+1,j}$. $\tilde{p}_{i+1,j}$ is given by the relation

$$\frac{p_{i+1,j} - \tilde{p}_{i+1,j}}{d(\mathbf{z}_{i+1,j}, \tilde{\mathbf{z}}_{i+1,j})} = \frac{p_{i+1,j} - p_{i+1,j-1}}{d(\mathbf{z}_{i+1,j}, \mathbf{z}_{i+1,j-1})}. \tag{20}$$

Therefore we approximate the first term on the right-hand side of Eq. (18) by

$$0.5h(f_{i,j} + f_{i+1,j})\,\kappa_b \frac{\tilde{p}_{i+1,j} - p_{i,j}}{d(\tilde{\mathbf{z}}_{i+1,j}, \mathbf{z}_{i,j})}, \tag{21}$$

where $\tilde{p}_{i+1,j}$ is given by (20).

The approximation of $\partial p((i+0.5)h, \xi_2)/\partial x$ in (17) is similar to the approximation done above. The term $\partial p((i+0.5)h, \xi_2)/\partial x$ in the equation is approximated by the difference quotient

$$\frac{p_{i+1,j} - \hat{p}_{i,j}}{d(\mathbf{z}_{i+1,j}, \hat{\mathbf{z}}_{i,j})}, \tag{22}$$

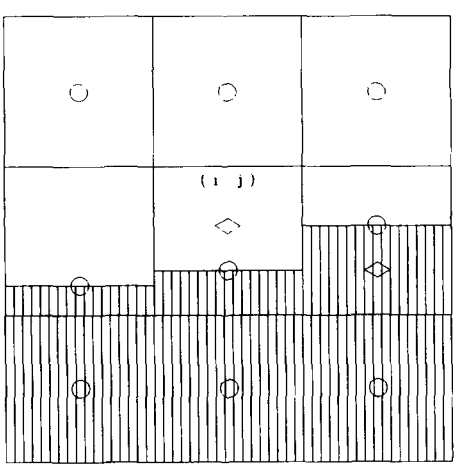

FIG. 5. Example of horizontal interface to be discretized. Circles denote location in cell where pressure is solved for. Diamonds denote where the pressure is to be approximated by interpolation.

where $\hat{p}_{i,j}$ represents an approximation to the grid function at $\hat{\mathbf{z}}_{i,j}$, a point in the white fluid, chosen on the line between $\mathbf{z}_{i,j}$ and $\mathbf{z}_{i,j+1}$, with the same y-coordinate as $\mathbf{z}_{i+1,j}$. The location of $\tilde{\mathbf{z}}_{i,j}$ is denoted by the diamond in Fig. 5 in cell (i, j). Using the same methodology above, $\hat{p}_{i,j}$ is given by the relation

$$\frac{\hat{p}_{i,j} - p_{i,j}}{d(\hat{\mathbf{z}}_{i,j}, \mathbf{z}_{i,j})} = \frac{p_{i,j+1} - p_{i,j}}{d(\mathbf{z}_{i,j+1}, \mathbf{z}_{i,j})}. \tag{23}$$

Therefore we approximate the second term on the right-hand side of Eq. (17) by

$$0.5h(2 - f_{i,j} - f_{i+1,j})\kappa_w \frac{p_{i+1,j} - \hat{p}_{i,j}}{d(\mathbf{z}_{i+1,j}, \hat{\mathbf{z}}_{i,j})}, \tag{24}$$

where $\hat{p}_{i,j}$ is given by (23). After summing the two terms in Eqs. (21) and (24), we have the approximation,

$$\begin{aligned}\int_{RS} \mathbf{u} \cdot \mathbf{n}\, ds \approx\ & 0.5h(f_{i,j} + f_{i+1,j})\, \kappa_b \frac{\tilde{p}_{i+1,j} - p_{i,j}}{d(\tilde{\mathbf{z}}_{i+1,j}, \mathbf{z}_{i,j})} \\ & + 0.5h(2 - f_{i,j} - f_{i+1,j})\, \kappa_w \frac{p_{i+1,j} - \hat{p}_{i,j}}{d(\mathbf{z}_{i+1,j}, \hat{\mathbf{z}}_{i,j})},\end{aligned} \tag{25}$$

where $\tilde{p}_{i+1,j}$ and $\hat{p}_{i,j}$ are given by (20) and (23), respectively.

There is no interface crossing the top side of cell (i, j), only white fluid. $\mathbf{u} \cdot \mathbf{n}$ simplifies on the top side to $\kappa_w(\partial p((x, (j+0.5)h)/\partial y)$. The line integral on the top side is approximated by

$$\int_{TS} \mathbf{u} \cdot \mathbf{n}\, ds \approx h\kappa_w \frac{p_{i,j+1} - p_{i,j}}{d(\mathbf{z}_{i,j+1}, \mathbf{z}_{i,j})}. \tag{26}$$

The line integral on the left side of cell (i, j) is discretized in a similar manner as the line integral on the right side. The line integral on the bottom side is done in a similar manner to the line integral over the top side. These discretizations are substituted in Eq. (13) to give an equation for the grid function value in cell (i, j) and its neighbors.

3.3. *Modified Conjugate Gradient Method*

To solve our system of equations for the unknown pressures obtained in Section 3.2, two versions of the conjugate gradient method are used. The first algorithm, presented by Concus *et al.* in [9], applies a preconditioned conjugate gradient method to the system

$$A\mathbf{x} = b. \tag{27}$$

Our second algorithm finds a least squares solution to (27) and is presented by Hestenes in [19]. Our matrix A does not satisfy all the conditions used in the

analysis of convergence of our first conjugate gradient algorithm. In particular, it is not symmetric because of the interpolation used in Section 3.2 and it is singular because of the periodic and Neumann boundary conditions. Therefore, for Algorithm 1, the norm of our residual

$$|A\mathbf{x}_k - b| \tag{28}$$

sometimes does not become small enough, where $\mathbf{x}_k$ is the kth approximate to $\mathbf{x}$ after iterating the conjugate gradient method k times. This is resolved by using Algorithm 2 to find a least squares solution for which (28) is less than our prescribed tolerance. Algorithm 2 requires many more multiplications than Algorithm 1. Algorithm 1 works so often that it is much cheaper to use Algorithm 1 with Algorithm 2 as a backup than using Algorithm 2 alone. Our preconditioner is chosen to be the discrete 5-point Laplacian matrix with Neumann boundary condi-

was obtained from the FISHPAK library [21].

3.4. *Surface Tension and Curvature*

Surface tension and curvature are included in our model in the following way. Our method is designed so that if an interface passes through a cell then we solve for the pressure at some prescribed point on this interface. For each cell containing an interface the unknown pressure in that cell is involved in computing the velocities in the white fluid and the black fluid. Whenever we are computing the velocity of the black fluid, instead of using $p_{i,j}$ as the pressure on the interface for the bottom fluid we use $p_{i,j} + \tau/R_{i,j}$, where $R_{i,j}$ is the estimated radius of curvature on the interface in cell (i, j). In computing the velocity in the white fluid, we use $p_{i,j}$. This only modifies the right side of Eq. (27). This does not treat the black and white fluids differently (see [34]).

The curvature is computed using a method due to Chorin in [5]. This method is designed for interfaces represented by volume fractions. Consider a cell (i, j) with a volume fraction $0 < f_{i,j} < 1$ and suppose we desire to estimate its curvature. The method uses the volume fractions of cell (i, j) and some of its neighbors. The main idea is to find a circle whose intersection with these cells cuts out the same volume fractions as those of cell (i, j) and its neighbors. This circle is identified with the osculating circle and its radius is taken to be the radius of curvature of the interface in cell (i, j).

4. Numerical Results for the Linearized Theory

In this section, numerical results are compared with the predictions of the linearized theory. In Section 4.1, we give the rate of growth for a small wave as predicted by the linearized theory along with a method for approximating the rate of growth for a small wave associated with the numerical method. In Section 4.2,

the numerical results are presented and compared with the results predicted by the linearized theory.

4.1. *Numerical Rate of Growth*

In [7, 30], it is shown that when the Hele–Shaw equations are satisfied on both sides of an interface, given by the equation

$$y = \varepsilon e^{inx}, \tag{29}$$

then the interface, after a short time Δt, evolves into an interface given by the equation

$$y = \varepsilon e^{\sigma \Delta t} e^{inx}. \tag{30}$$

The analysis assumes that $\varepsilon e^{\sigma \Delta t}$ is small enough. The rate of growth σ is given by

$$\sigma = \frac{(\mu_w - \mu_b) Vn - \tau k n^3}{\mu_w + \mu_b}. \tag{31}$$

n is the wave number, ε is a small parameter, τ is the surface tension coefficient, $(0, V)$ is the velocity far ahead and far behind the interface, and $k = b^2/12$.

Our interface is evolved in a rectangular box in the $x - y$ plane as described in Section 2. The vertices of this rectangle are $(0, 0)$, $(1, 0)$, $(0, c)$, and $(1, c)$. The equation for the interface lying in the middle of the rectangle is

$$y = \varepsilon \cos(2nx) + c/2. \tag{32}$$

We choose n to be of the form $n_0 \pi$ for some integer n_0. A numerical grid is superposed over the rectangle with cells of dimension $h \times h$. There are m cells across horizontally and l cells vertically such that $m \cdot h = 1$ and $l/m = c$, where m and l are integers. l is assumed to be even for convenience. The interface lies in the center of the grid in the j_0 row of cells, where $j_0 = l/2 + 1$. This is accomplished by choosing ε small enough. To transform the interface represented by a curve into one represented by volume fractions, the following is done. A cell (i, j) has volume fraction $f_{i,j} = 1$ when it lies behind the interface (i.e., when $j < j_0$), volume fraction $f_{i,j} = 0$ when it lies in front of the interface (i.e., when $j > j_0$), and volume fraction $0 < f_{i,j} < 1$ when the interface passes through the cell (i.e., when $j = j_0$). For cells (i, j_0), where $i = 1, \ldots, m$, the amount of black fluid in the area lying in each cell is

$$a_{i,j_0} = \int_{(i-1)h}^{ih} \left(\varepsilon \cos(nx) + \frac{c}{2} - (j_0 - 1)h \right) dx. \tag{33}$$

The fraction of black fluid in each cell, f_{ij_0}, $i = 1, \ldots, m$ is given by

$$f_{ij_0} = a_{ij_0}/h^2. \tag{34}$$

Each cell in the j_0 row is then assumed to contain a horizontal interface with height $f_{ij_0}h$. The interface is viewed globally as a piecewise constant function given by

$$f(x) = f_{ij_0}h + (j_0 - 0.5)h \qquad \text{for} \quad (i-1)h \leqslant x \leqslant ih. \tag{35}$$

Our numerical method is applied to the interface represented by the volume fractions above. This gives a new interface represented by a new set of volume fractions. The new set of volume fractions correspond similarly to a piecewise constant function. We approximate the rate of growth of the cosine wave with wavenumber n by the rate of growth of the corresponding Fourier component of $f(x)$ with wavenumber n.

4.2. *Numerical Results*

The interface on our numerical grid is represented by the wave given by Eq. (32). The vertical dimension of the rectangle, c, is 1 and the velocity prescribed at the two horizontal sides is the constant 1. A wave, of amplitude 0.005, is evolved for a short time $\Delta t = 0.00001$ on our grid. Results are shown for wavenumbers $n = \pi$, 2π, ..., 9π and grid sizes of 20×20, 40×40, 60×60, and 80×80. Table I presents a comparison of the numerical σ with that predicted by the linearized theory for a surface tension coefficient of 10. The viscosity in the white fluid is 4 and the viscosity in the black fluid is 1. Results are given in Table II for a surface tension coefficient of 3. The results are similar when the values of the two viscosities are interchanged.

In general, our method relies on representing the interface as a piecewise constant function. The more oscillatory the interface, the harder it is to represent it on a

TABLE I

Growth Rates of Interfaces of the Form $\varepsilon \cos(2n\pi x)$

n	Numerical grid(20x20)	Numerical grid(40x40)	Numerical grid(60x60)	Numerical grid(80x80)	Linearized Prediction
1	3.525	3.432	3.176	2.944	3.435
2	5.377	4.945	4.861	4.809	4.861
3	3.338	2.524	2.341	2.318	2.268
4	-4.581	-6.139	-6.107	-6.288	-6.352
5	-20.117	-23.692	-23.218	-22.979	-23.009
6	-41.079	-52.254	-50.895	-49.879	-49.712
7	-64.794	-93.645	-91.279	-89.118	-88.470
8	-86.650	-148.693	-146.559	-142.690	-141.293
9	-101.916	-218.403	-218.141	-212.087	-210.189

Note. $\mu_a = 4$, $\mu_b = 1$, surface tension = 10, $\varepsilon = 0.005$, $\Delta t = 0.00001$.

TABLE II

Growth Rates of Interfaces of the Form $\varepsilon \cos(2n\pi x)$

n	Numerical grid(20x20)	Numerical grid(40x40)	Numerical grid(60x60)	Numerical grid(80x80)	Linearized Prediction
1	3.769	3.669	3.584	3.512	3.669
2	7.357	6.855	6.751	6.718	6.736
3	9.981	8.926	8.663	8.595	8.597
4	10.960	9.286	8.666	8.671	8.650
5	9.866	7.409	6.736	6.494	6.292
6	7.664	2.950	1.930	1.598	0.920
7	4.502	-5.013	-6.583	-6.976	-8.069
8	1.348	-17.373	-19.595	-19.873	-21.276
9	-1.316	-33.913	-37.330	-37.415	-39.306

Note. $\mu_w = 4$, $\mu_b = 1$, surface tension = 3, $\varepsilon = 0.005$, $\Delta t = 0.00001$.

fixed grid. The numerical predictions of the linearized theory in Tables I and II are therefore not as good for higher wavenumbers.

In Fig. 6, we show a plot of σ versus μ_w/μ_b, where $\mu_b = 1$ and $\mu_w \geqslant 1$. The surface tension coefficient is 3 and the computations are done on a 40×40 grid. In Fig. 7, we show a plot of σ versus surface tension, where $\mu_w = 1.3$ and $\mu_b = 1.0$. In Fig. 6

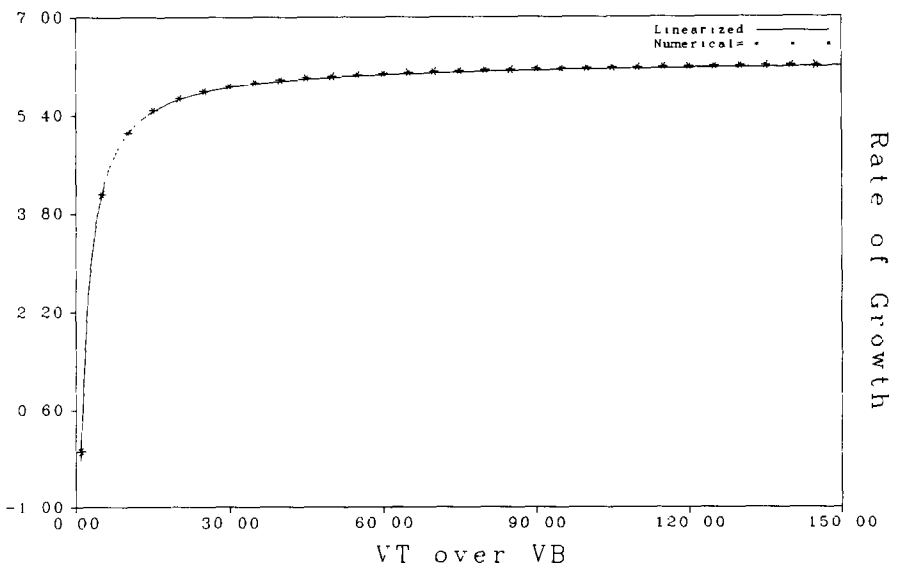

FIG. 6. The rate ot growth of a cosine wave versus the viscosity ratio. The predictions of the linearized theory are compared with the numerical results when μ_w is greater than μ_b and the surface tension is 3. The initial perturbation is a cosine wave with wavenumber 2π. The time step is 0.0001, the wave has an amplitude of 0.0001 and the interface is evolved on a 40×40 grid.

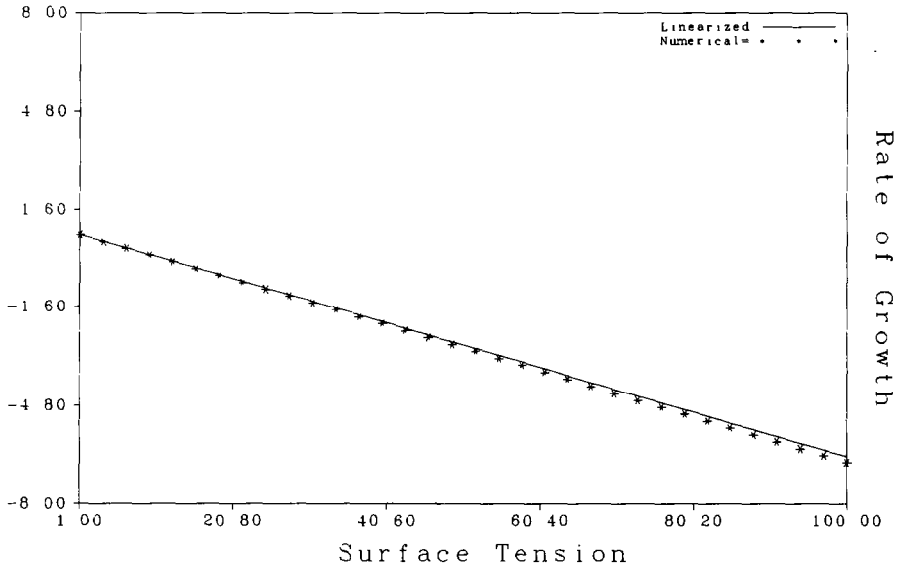

FIG. 7. The rate of growth of a consine wave versus surface tension. The predictions of the linearized theory are compared with the numerical results when $\mu_w = 1.3$ and $\mu_b = 1$. The initial perturbation is a cosine wave with wavenumber 2π. The time step is 0.0001, the wave has an amplitude of 0.005 and the interface is evolved on a 40×40 grid.

and 7, the time step Δt is 0.0001, computations are done on a 40×40 grid, and the wavenumber, n, is π.

For Tables I and II, the interface remains inside one row of cells over one time step. We now consider the numerical rate of growth at each time step for an evolving interface. This interface eventually is contained in 10 rows of cells. We start with an interface given by a cosine wave with amplitude 0.01 and wavenumber π in the middle row of cells. This interface is allowed to evolve according to our numerical method with a constant time step 0.00333. At each time step, the numerical rate of growth is calculated and shown along with the rate of growth predicted by the linearized theory. In addition, we have the coefficient (amplitude) of the cosine term of the Fourier series of wavenumber π along with the number of rows of cells containing the interface. The results are for a surface tension coefficient of 5 on a 40×40 grid with $\mu_w = 4$ and $\mu_b = 1$. Results are shown for every 10 time steps up to the first 190 and for every time step for iterations 190 through 200. These results are presented in Table III. As the amplitude increases, the results show a steady decrease in the numerical rate of growth from the result predicted by the linearized theory until about iteration 190 when the value begins to oscillate rapidly. We attribute this to the violation of an assumption of the linearized theory, i.e., that the wave has small amplitude. However, further experiments are required to validate this.

The same experiment is run with a 2π wave and all other parameters the same

TABLE III

Growth Rates of an Evolving Interface Initially of the Form $0.01 \cdot \cos(2\pi x)$

Iteration Number	Amplitude	Numerical σ	Linearized σ	Rows of cells with interface
1	0.0100	3.583	3.602	1
20	0.0126	3.579	3.602	2
40	0.0160	3.589	3.602	3
60	0.0202	3.570	3.602	3
80	0.0256	3.512	3.602	3
100	0.0324	3.525	3.602	3
120	0.0409	3.495	3.602	4
140	0.0515	3.469	3.602	6
160	0.0648	3.499	3.602	6
180	0.0813	3.376	3.602	7
190	0.0906	3.743	3.602	8
191	0.0916	3.508	3.602	8

as above. The results are shown for every 5 time steps up to 70 and for every time step for iterations 70–77. As the amplitude increases, a similar decrease in the numerical rate of growth is observed followed by a similar oscilatory behavior. These results are shown in Table IV.

In solving our system of equations given by (27), we require that

$$|\mathbf{b} - A\mathbf{x}|_{\infty} < 0.0001, \tag{36}$$

where $\|_{\infty}$ denotes the maximum norm and $\mathbf{x}$ is the vector of grid function values for the pressure. Only the first version of the modified conjugate gradient algorithm is ever needed. About 23 iterations are required to satisfy (36) when $\mu_w = 4$ and $\mu_b = 1$. The number of iterations increase as the viscosity ratio increases.

The curvature algorithm attempts to find the radius r of the osculating circle. The algorithm only considers circles with radii less than some prescribed radius $r_0 > 0$. For cells with radius of curvature, in absolute value, greater than r_0, the value of

TABLE IV

Growth Rates of an Evolving Interface Initially of the Form $0.01 \cdot \cos(2\pi x)$

Iteration Number	Amplitude	Numerical σ	Linearized σ	Rows of cells with interface
1	0.0101	6.181	6.200	1
5	0.0109	6.161	6.200	2
10	0.0121	6.188	6.200	2
15	0.0134	5.967	6.200	2
20	0.0148	6.094	6.200	2
25	0.0164	6.153	6.200	3
30	0.0181	6.129	6.200	2
35	0.0200	6.034	6.200	2
40	0.0222	6.072	6.200	3
45	0.0244	5.921	6.200	3
50	0.0270	6.068	6.200	3
55	0.0297	5.805	6.200	3
60	0.0328	5.263	6.200	4
65	0.0362	6.041	6.200	4
70	0.0399	5.727	6.200	4
71	0.0407	6.157	6.200	4
72	0.0415	5.783	6.200	4
73	0.0423	5.883	6.200	4
74	0.0431	5.912	6.200	4
75	0.0435	2.694	6.200	4
76	0.0422	-8.749	6.200	5
77	0.0438	11.278	6.200	5

Note. $\mu_u = 4$, $\mu_b = 1$, time step $= 0.00333$, $\tau = 5$ on a 40×40 grid.

zero is given for the curvature. Our r_0 is chosen to be 1000. Our numerical method cannot expect to do well for waves with curvature less than $\frac{1}{1000}$. By choosing a larger amplitude, the region where the curvature is less than $\frac{1}{1000}$ becomes smaller. This is why our amplitude can not be choosen much smaller than 0.005.

5. Numerical Results for Finite Amplitude Perturbations

In this section, we apply the numerical method to interfaces of finite amplitude.

Our interface is evolved in a rectangular box in the $x - y$ plane, as described in Section 2. The four corners of the rectangular box lie at (0, 0), (1, 0), (0, 2), and (1, 2). The velocity prescribed on the horizontal sides is again 1. There are m cells across horizontally and l cells vertically such that $m \cdot h = 1$ and $1/m = 2$, where m and

I are integers. Our interface is initially a *sin* wave of small amplitude. This interface is converted to its corresponding volume fraction representation. The numerical method is applied to the interface and an updated set of volume fractions is obtained as done in Section 4. The interface is evolved by successively applying the numerical method to the updated set of volume fractions. Results are presented below for several values of the surface tension coefficient.

All computations are done on a 30×60 grid with $\mu_w = 4$ and $\mu_b = 1$. The interface given by the volume fractions above is evolved in Fig. 8 for the case of a surface tension coefficient of 3. The interface is evolved over a period of time $t = 1.69$ s (210 time steps). In Fig. 9, we evolve the interface with a surface tension of 7. It is evolved over a period of time $t = 1.97$ s (230 time steps). In Fig. 10, we evolve the interface with a surface tension of 14. It is evolved over a period of time $t = 1.91$ s (370 time steps). Figures 8, 9, and 10 are obtained by shading in each cell (i, j), where $f_{i,j} > 0$. To reduce the effects of the horizontal boundaries, after each time step the interface is translated back to the middle of the grid.

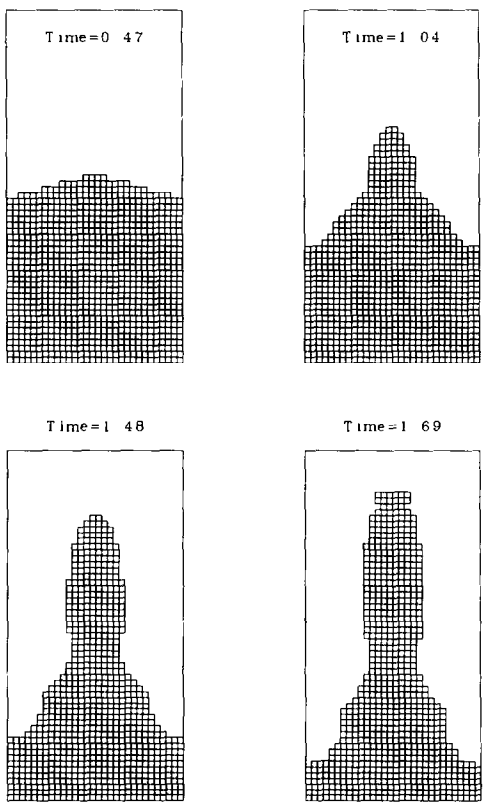

FIG. 8. A *sin* wave is evolved and the interface is shown at times 0.47, 1.04, 1.48, and 1.69 s. A surface tension of 3 is used, $\mu_w = 4$, $\mu_b = 1$, and a 30×60 grid is used.

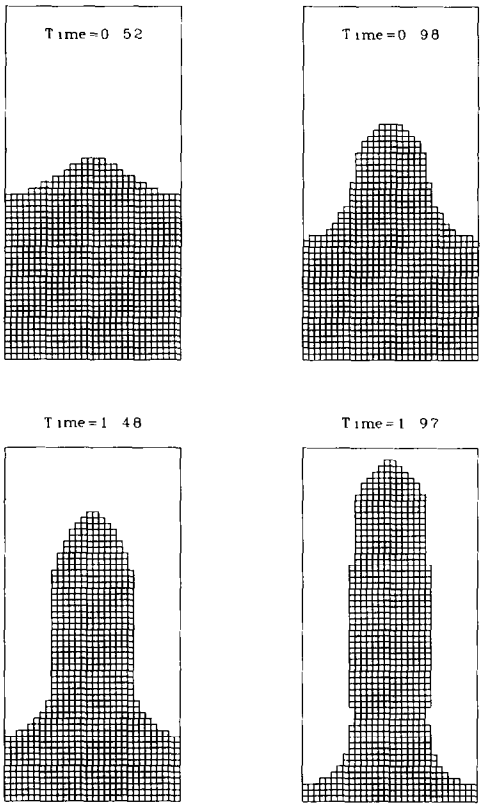

FIG. 9. A sin wave evolved and the interface is shown at times 0.52, 0.98, 1.48, and 1.97 s. A surface tension of 7 is used, $\mu_w = 4$, $\mu_h = 1$, and a 30×60 grid is used.

Our numerical method for advecting the flow satisfies a Courant–Friedrichs–Lewy condition that

$$\frac{\Delta t}{h} \leqslant \frac{1}{|U|}, \tag{37}$$

where $|U|$ is the maximum speed of the flow and Δt is the time step. We choose

$$\Delta t = \frac{h}{2|U|} \tag{38}$$

as our time step.

In the first conjugate gradient method, our residual sometimes does not become small enough. After 100 iterations of the first algorithm, we use the second algorithm. We required the residual to be smaller than 0.0001.

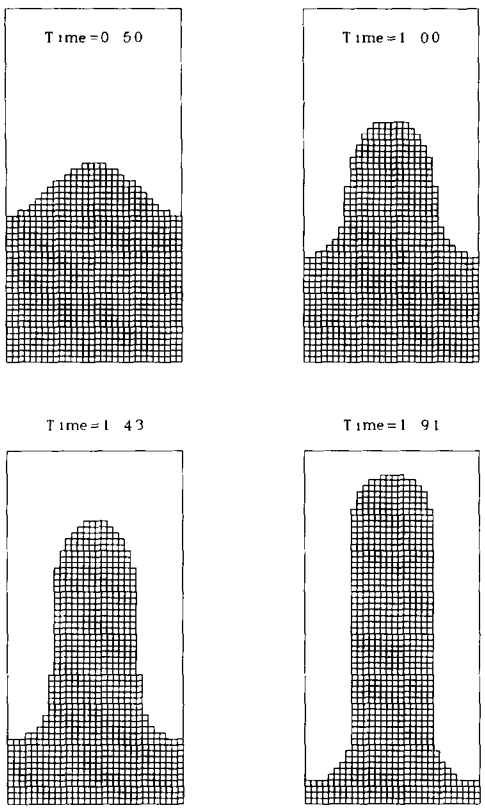

FIG. 10. A *sin* wave evolved and the interface is shown at times 0.50, 1.00, 1.43, and 1.91 s. A surface tension of 14 is used, $\mu_w = 4$, $\mu_b = 1$, and a 30×60 grid is used.

In discretizing the weak formulation of the continuity equation to find the velocity field, a local reconstruction of the interface in each cell is required. We examine the volume fractions in the cell and its neighbors and determining the interface for that situation. We do not include every configuration of volume fractions in Section 3.1. Occasionally a configuration of volume fractions appears which is not covered in Section 3.1. This happens either because the interface is too complex to be represented by the simple structures in Section 3.1 or because of numerical instabilities. It happens no more than once in every 30 time steps. It is probably possible to design a version of our algorithm to handle all possible cases but we choose not to do so here. It would require using more complicated structures than just horizontal lines, vertical lines, and corners. Our numerical experiments seem to indicate that as the surface tension becomes smaller, the interface becomes less smooth and the chances of encountering a situation not covered increases. When a configuration results that is not covered by Section 3.1, the following is done. We look for cells (i, j) the are partially full with none of its neighbors full, i.e., the eight

cells sharing a side or a corner with cell (i, j). We assign the amount of black fluid in cell (i, j) to the neighboring cell whose volume fraction is the largest. When the amount added to the neighboring cell makes its volume fraction greater than one, then the volume fraction of the neighbor is forced to be one and cell (i, j) gets the residual. This is one of many possible remedies.

This version of our code assumes symmetry about the center of the cell. The results are qualitatively similar to the results of McLean and Saffman [23]. They will be compared quantitatively later. Our results are also similar to experimental results observed in the laboratory (see Saffman and Taylor [30]; Chuoke *et al.* [7]) and to other numerical results (see Meng and Thomson [25]; Tryggvason and Aref [32, 33]; Degregoria and Schwartz [11, 12]; Meiburg and Homsy [24]). The fingers which we observe are rounded at the ends with thin necks. Surface tension tends to fatten the fingers. At low surface tensions, the interface is also less smooth.

We will also study grid effects of our numerical method later. The growth of fingers and grid effects for a slightly different equation are studied in [17, 14].

6. Conclusions

A numerical method is presented for evolving an interface between two immiscible fluids in a Hele–Shaw cell. Our numerical method is applied to waves of small amplitude for a wide range of wavenumbers and surface tensions. Good agreement is found between our numerical rates of growth and the rates of growth as predicted by the linearized theory. The linearized theory acts as a test problem for the numerical method. By solving this problem with some accuracy, one might expect acceptable results for finite amplitude waves. Our results for finite amplitude perturbations are qualitatively similar to results of experiments and other numerical results.

We did not give rationale for our choice of where to solve for the grid function in each cell in Section 3.2. We made our choices attempting to get the most accurate difference approximations and to minimize interpolation.

For our numerical method, the horizontal interface and vertex corners are used mostly in describing small amplitude waves. The numerical results of the linearized theory seem to justify the choices for those interfaces. One might expect the same for the vertical interfaces. It seems that the corner can only be tested for a nonlinear solution. In the future, we plan to compare our results to the McLean and Saffman steady fingers which should provide a good test for the corners.

Acknowledgments

I first thank Alexandre Chorin for his encouragement and enthusiastic interest in my work. I also thank Paul Concus, Christoph Borgers, and John Strain for helpful discussions. These calculations were performed at the Lawrence Berkeley Lab, University of California and at the Mathematics and Statistics Department, University of Massachusetts.

REFERENCES

1. J. M. AITCHISON AND S. D. HOWISON, *J. Comput. Phys.* **60**, 376 (1985).
2. J. BEAR, *Dynamics of Fluids in Porous Media* (Elsevier, New York, 1972).
3. A. J. CHORIN, *J. Comput. Phys.* **35**, 1 (1980).
4. A. J. CHORIN, *Commun. Math. Phys.* **91**, 103 (1983).
5. A. J. CHORIN, *J. Comput. Phys.* **57**, 472 (1985).
6. J. P. CHRISTENSEN, *J. Comput. Phys.* **13**, 363 (1973).
7. R. L. CHUOKE, P. VAN MEURS, AND C. VAN DER POEL, *Trans. Amer. Inst. Min. Eng.* **AIME-216**, 188 (1959).
8. P. COLELLA, P. CONCUS, AND J. SETHIAN, "Some numerical methods for discontinuous flows in porous media," *The Mathematics of Reservoir Simulation*, edited by R. E. Ewing (SIAM, Philadelphia, 1983), p. 161.
9. P. CONCUS, G. H. GOLUB, AND D. P. O'LEARY,"A generalized conjugate gradient method for the numerical solution of elliptic partial differential equations," *Sparse Matrix Computations*, edited by J. R. Bunch and J. Roses (Academic Press, New York, 1976), p. 302.
10. P. CONCUS AND W. PROSKUROWSKI, *J. Comput. Phys.* **30**, 153 (1979).
11. A. J. DEGREGORIA AND L. W. SCHWARTZ, *Phys. Fluids* **28**, 2313 (1985).
12. A. J. DEGREGORIA AND L. W. SCHWARTZ, *J. Fluid Mech.* **164**, 383 (1986).
13. A. F. GHONIEM, A. J. CHORIN, AND A. K. OPPENHEIM, *Philos. Trans. Roy. Soc. London Ser. A* **304**, 303 (1982).
14. J. GLIMM, ISAACSON, D. MARCHESIN, AND O. MCBRYAN, *Adv. Appl. Math.* **2**, 91 (1981).
15. J. GLIMM, D. MARCHESIN, AND O. MCBRYAN, *Commun. Math. Phys.* **74**, 1 (1980).
16. J. GLIMM, D. MARCHESIN, AND O. MCBRYAN, *J. Comput. Phys.* **38**, 179 (1981).
17. J. GLIMM, D. MARCHESIN, AND O. MCBRYAN, *Commun. Pure Appl. Math.* **24**, 53 (1981).
18. S. P. GUPTA, J. E. VARNON, AND R. A. GREENKORN, *Water Resources Res.* **19**, 1039 (1973).
19. M. R. HESTENES, *Conjugate Direction Methods in Optimization* (Springer-Verlag, New York, 1980).
20. H. LAMB, *Hydrodynamics* (Cambridge Univ. Press, Cambridge, 1932).
21. FISHPAK Library, The National Center for Atmospheric Research, Boulder, Co, 1980 (unpublished).
22. P. LOTSTEDT, *J. Comput. Phys.* **47**, 211 (1982).
23. J. W. MCLEAN AND P. G. SAFFMAN, *J. Fluid Mech.* **102**, 455 (1981).
24. E. MEIBURG AND G. M. HOMSY, *Phys. Fluids* **31**, 429 (1988).
25. J. C. S. MENG AND J. A. L. THOMSON, *J. Fluid Mech.* **84**, 433 (1978).
26. W. NOH AND P. WOODWARD, in *Proceedings, Fifth International Conference on Fluid Mechanics*, edited by A. I. van de Vooran and P. J. Zandberger (Springer-Verlag, New York, 1976).
27. C.-W. PARK, S. GORELL, AND G. M. HOMSY, *J. Fluid Mech.* **141**, 257 (1984).
28. L. PATERSON, *J. Fluid Mech.* **113**, 513 (1981).
29. E. PITTS, *J. Fluid Mech.* **97**, 53 (1980).
30. P. G. SAFFMAN AND G. I. TAYLOR, *Proc. Roy. Soc. London* **245**, 312 (1958).
31. J. A. SETHIAN, *J. Comput. Phys.* **55**, 425 (1984).
32. G. TRYGGVASON AND H. AREF, *J. Fluid Mech.* **136**, 1 (1983).
33. G. TRYGGVASON AND H. AREF, *J. Fluid Mech.* **154**, 287 (1985).
34. N. WHITAKER, Thesis, University of California, Berkeley, 1987 (unpublished).
35. I. WHITE, P. M. COLOMBERA, AND J. R. PHILIP, *Soil Sci. Soc. Amer. J.* **40**, 824 (1976).
36. I. WHITE, P. M. COLOMBERA, AND J. R. PHILIP, *Soil Sci. Soc. Amer. J.* **41**, 483 (1977).